



This paper is a part of the hereunder thematic dossier published in OGST Journal, Vol. 69, No. 6, pp. 977-1129 and available online [here](#)

Cet article fait partie du dossier thématique ci-dessous publié dans la revue OGST, Vol. 69, n°6, pp. 977-1129 et téléchargeable [ici](#)

DOSSIER Edited by/Sous la direction de : **P.-L. Carrette**

PART 2

Post Combustion CO₂ Capture Captage de CO₂ en postcombustion

Oil & Gas Science and Technology – Rev. IFP Energies nouvelles, Vol. 69 (2014), No. 6, pp. 977-1129

Copyright © 2014, IFP Energies nouvelles

- 977 > Editorial
- 989 > *Post-Combustion CO₂ Capture by Vacuum Swing Adsorption Using Zeolites – a Feasibility Study*
Captage du CO₂ en postcombustion par adsorption modulée en pression avec désorption sous vide sur zéolithes — étude de faisabilité
G. D. Pirngruber, V. Carlier and D. Leinekugel-le-Cocq
- 1005 > *Membrane Separation Processes for Post-Combustion Carbon Dioxide Capture: State of the Art and Critical Overview*
Procédés membranaires pour le captage du dioxyde de carbone : état de l'art et revue critique
B. Belaisaoui and É. Favre
- 1021 > *Pressure Drop, Capacity and Mass Transfer Area Requirements for Post-Combustion Carbon Capture by Solvents*
Pertes de charge, capacité et aires de transfert de matière requises pour le captage du CO₂ en postcombustion par solvants
A. Lassauce, P. Alix, L. Raynal, A. Royon-Lebeaud and Y. Haroun
- 1035 > *Hollow Fiber Membrane Contactors for Post-Combustion CO₂ Capture: A Scale-Up Study from Laboratory to Pilot Plant*
Captage postcombustion du CO₂ par des contacteurs membranaires de fibres creuses : de l'échelle laboratoire à l'échelle pilote industriel
É. Chabanon, E. Kimball, É. Favre, O. Lorain, E. Goetheer, D. Ferre, A. Gomez and P. Broutin
- 1047 > *Hollow Fiber Membrane Contactors for CO₂ Capture: Modeling and Up-Scaling to CO₂ Capture for an 800 MW_e Coal Power Station*
Contacteurs à membrane à fibres creuses pour la capture de CO₂ : modélisation et mise à l'échelle de la capture du CO₂ d'une centrale électrique au charbon de 800 MW_e
E. Kimball, A. Al-Azki, A. Gomez, E. Goetheer, N. Booth, D. Adams and D. Ferre
- 1059 > *Regeneration of Alkanolamine Solutions in Membrane Contactor Based on Novel Polynorbornene*
Régénération de solutions d'alcanolamine dans un contacteur à membrane basé sur un nouveau polynorbornène
A.A. Shutova, A.N. Trusov, M.V. Bermeshev, S.A. Legkov, M.L. Gringolts, E.Sh. Finkelstein, G.N. Bondarenko and A.V. Volkov
- 1069 > *Development of HiCapt+™ Process for CO₂ Capture from Lab to Industrial Pilot Plant*
Développement du procédé HiCapt+™ pour le captage du CO₂ : du laboratoire au pilote industriel
É. Lemaire, P. A. Bouillon and K. Lettat
- 1081 > *A Technical and Economical Evaluation of CO₂ Capture from Fluidized Catalytic Cracking (FCC) Flue Gas*
Évaluation technico-économique du captage du CO₂ présent dans les fumées d'une unité FCC (*Fluidized Catalytic Cracking*)
R. Digne, F. Feugnet and A. Gomez
- 1091 > *Pilot Plant Studies for CO₂ Capture from Waste Incinerator Flue Gas Using MEA Based Solvent*
Étude du captage du CO₂ dans des gaz de combustion d'un incinérateur de déchets à l'aide d'un pilote utilisant un solvant à base de MEA
I. Aouini, A. Ledoux, L. Estel and S. Mary
- 1105 > *Amine Solvent Regeneration for CO₂ Capture Using Geothermal Energy with Advanced Stripper Configurations*
Régénération d'un solvant de captage du CO₂ utilisant l'énergie géothermique et des configurations améliorées pour le régénérateur
D.H. Van Wagener, A. Gupta, G.T. Rochelle and S.L. Bryant
- 1121 > *ACACIA Project – Development of a Post-Combustion CO₂ capture process. Case of the DMX™ process*
Projet ACACIA – Développement d'un procédé de captage du CO₂ postcombustion – Cas du procédé DMX™
A. Gomez, P. Briot, L. Raynal, P. Broutin, M. Gimenez, M. Soazic, P. Cessat and S. Saisset

Pressure Drop, Capacity and Mass Transfer Area Requirements for Post-Combustion Carbon Capture by Solvents

A. Lassauce, P. Alix*, L. Raynal, A. Royon-Lebeaud and Y. Haroun

IFP Energies nouvelles, Rond-point de l'échangeur de Solaize, BP 3, 69360 Solaize - France

e-mail: aurelia.lassauce@ifpen.fr - pascal.alix@ifpen.fr - ludovic.raynal@ifpen.fr - aude.royon-lebeaud@ifpen.fr - yacine.haroun@ifpen.fr

* Corresponding author

Résumé — Pertes de charge, capacité et aires de transfert de matière requises pour le captage du CO₂ en post-combustion par solvants — Les procédés de captage en post-combustion utilisant des amines sont considérés comme l'une des options préférées pour le captage et le stockage du CO₂ (CSC, *CO₂ Capture and Storage*). Cependant, le coût du CO₂ évité est très important et doit être réduit. Ce coût est fortement lié aux designs des colonnes, qui doivent, par conséquent, être optimisées. Dans cet article, les performances hydrodynamiques et le transfert de matière de garnissages vrac et structurés sont discutés en terme de perte de charge, de capacité et, le plus important, en terme de coefficients de transfert de matière, notamment l'aire interfaciale, paramètre le plus important pour la conception d'absorbants de CO₂. La comparaison de différents garnissages commerciaux à haute efficacité est discutée à partir de caractérisations expérimentales et de simulations CFD et une méthodologie pour de futurs développements est proposée.

Abstract — Pressure Drop, Capacity and Mass Transfer Area Requirements for Post-Combustion Carbon Capture by Solvents — *Post-combustion capture processes using amines are considered as one of the preferred options for CO₂ Capture and Storage (CCS). However, the cost of avoided CO₂ is very large and must be reduced. The latter cost is strongly linked with column designs which consequently must be optimized. In the present article, hydrodynamics and mass transfer performances of random and structured packings are discussed in terms of pressure drop, capacity and most importantly in terms of mass transfer parameters, in particular in terms of interfacial area which is the most important parameter for CO₂ absorbers design. Comparison of different commercial high efficiency packings is discussed from experimental characterization and from CFD simulations and a methodology for future developments is proposed.*

INTRODUCTION

Post-combustion CO₂ capture processes using amines are considered as one of the preferred options for CO₂ Capture and Storage (CCS). However, the cost of avoided CO₂ is very large and must be reduced. The latter cost is strongly linked with column designs which consequently must be optimized.

Since capture process operates downstream the power plant, it requires very low pressure drop. For the absorber, the overall pressure drop, including the inlet and the outlet of the column, should be minimum and at least less than 100 mbar. To meet these requirements of size optimization and pressure drop limitation, efficient high capacity packings are needed. This is the main reason why the IMTP 50 random packing has been replaced by the Mellapak 2X structured packing on the Esjberg pilot plant (Knudsen, 2009). However, this choice can be discussed: indeed, achieving a high interfacial area is at least as important as achieving low pressure drop and, as shown for IMTP random packings by Raynal *et al.* (2013). One may prefer to use a more efficient packing leading to larger diameter columns but also leading to smaller packed bed height resulting in a reduction of total volume further resulting in a reduced investment. This is the reason why the highly efficient Mellapak 350.X structured packing has been considered in the present study even if less capacitive than the Mellapak 2X structured packing.

To build up models that will be used for columns design, tests are needed to characterize these packings in terms of hydrodynamics and mass transfer. The aim of the present article is to show and discuss hydrodynamics and mass transfer performances of random and structured packings in terms of pressure drop, capacity and mass transfer parameters. Assuming MonoEthanol-Amine (MEA) 30 wt% as the base case process for CO₂ post-combustion capture (Knudsen *et al.*, 2006; Feron *et al.*, 2007), one can consider that fast reactions will occur in capture plants and that the interfacial area, a_e , is the main parameter to estimate the efficiency of an absorber (Danckwerts, 1970; Raynal *et al.*, 2013).

In the following, a non exhaustive review presents experimental set-ups and methods used by different authors about packings that we consider of interest. Those packings are first the IMTP50 and the Mellapak 2X, because they have been used in the CASTOR¹ pilot and, thus, can be considered as reference packings (Knudsen, 2009). Second, to complete the random packings of reference, IMTP (2003) and similar I-Ring random packings should be considered. Last, the Mellapak

series, or equivalent, structured packings are of interest, because they are well documented in the literature and offer both high geometric areas and low pressure drops (Spiegel and Meier, 1992). In these Mellapak series structured packings, it has been considered, in the present study, that the Mellapak 350.X which is more interesting in terms of efficiency than in terms of capacity, should also be studied.

Experimental tools and methods available at IFP Energies nouvelles (IFPEN) are briefly described. Third, results are shown and discussed in terms of dry and wetted pressure drop, flooding limit and effective area. Finally, some CFD modeling results are presented, the possibility to predict hydrodynamics and mass transfer performances for the development of future geometries is then discussed.

1 LITERATURE REVIEW

A lot of authors have performed pressure drop and interfacial area measurements with random and/or structured packings in countercurrent flow. Geometric characteristics of random packings studied are given in Table 1 and those of structured packings are given in Table 2. It has to be underlined that Mellapak 2X is not listed in Table 2 in spite of the fact that it has been used in the CASTOR pilot plant. This is explained by the fact that no experimental data is available in terms of interfacial area for this packing. However, there are enough data to propose a general correlation for further process studies (see Sect. 3).

Concerning hydrodynamics performances of random packings, Kehrer *et al.* (2006) have performed experiments with the I-Ring random packings, from I-Ring#15 to #70, with the air-water system at medium to high liquid loads in the Sulzer Chemtech facilities. Only pressure drop measurements have been performed. A smaller air-water column of inner diameter 0.25 m was used to measure the experimental data points for I-Ring size #15, whereas an industrial sized air-water column with an inner diameter of 1 m was used to obtain experimental data points for I-Ring sizes #40 to #70. The height of the packed bed is 2.05 m for the I-Ring#15, 3.05 m for I-Ring#40, 4.5 m for I-Ring#50 and 2.94 m for I-Ring#70. In the air-water columns, the two phases ran under ambient conditions (atmospheric pressure, ambient temperature) and a Sulzer VKG (channel distributor with ground holes; integrated arm channels and main trough) has been used as distributor type. The authors give no information about the drip point density of the liquid distributor. Liquid load, Q_L , was varied from 0 to 60 m³/m²/h for I-Ring#15, from 0 to

¹ www.co2-castor.com

TABLE 1
Geometric characteristics of random packings studied

Random packings	I-Ring#15	I-Ring#25	I-Ring#40	I-Ring#50	I-Ring#50	I-Ring#70	IMTP25	IMTP40	IMTP50	IMTP50	RSR 1.5	RMSR 50
References	Kehrer et al. (2006)	Present work	Kehrer et al. (2006)	Seibert et al. (2005)	Seibert et al. (2005)	Nakov et al. (2007)	Alix and Raynal (2009)	Nakov et al. (2007)	Linek et al. (2001)			
Packed bed height (m)	2.05	NA	3.05	4.5	1.38	2.94	3.3	3.3	2.4	1.5	2.4	1.2
Column inner diameter (m)	0.25	NA	1	1	0.4	1	0.43	0.43	0.47	0.4/1.1	0.47	0.29
Geometric area (m ² /m ³)	290	230	150	100	112	60	NA	NA	107.1	110	105.8	86 (Rauschert: 115)

TABLE 2
Geometric characteristics of structured packings studied

Structured packings	Montz B1-250	Montz A3-500	Montz B1-500	Mellapak 125.X	Mellapak 125.Y	Mellapak 2Y	Mellapak 250.X	Mellapak 250.X	Mellapak 250.Y	Mellapak 250.Y	Mellapak 350.X	Mellapak 500.Y	Mellapak 500.Y
References	Seibert et al. (2005)	Seibert et al. (2005)	Seibert et al. (2005)	Spiegel and Meier (1992)	Tsai (2010)	Tsai (2010)	Spiegel and Meier (1992, 1994)	Tsai et al. (2011)	Spiegel and Meier (1992, 1994)	Tsai et al. (2011)	Present work	Tsai et al. (2011)	Spiegel and Meier (1994)
Packed bed height (m)	3.3	3.3	3.3	NA	3	3	NA	3	NA	3	1.13	3	NA
Column inner diameter (m)	0.43	0.43	0.43	1	0.43	0.43	1	0.43	1	0.43	0.4	0.43	1
Geometric area (m ² /m ³)	250	500	500	125	125	205	250	250	250	250	350	500	500
Channel angle/channel flow angle from horizontal (°)	NA	NA	NA	60	45	45	60	60	45	45	60	45	45

180 m³/m²/h for I-Ring#40 and I-Ring#50, and from 0 to 150 m³/m²/h for I-Ring#70. F -Factor $F_s = \sqrt{\rho_G} \times V_{SG}$ varying from 0 to 5 Pa^{0.5}, where ρ_G is the gas density and V_{SG} is the superficial gas velocity.

Alix and Raynal (2009) have studied hydrodynamic and mass transfer performances of IMTP50 random packing in two different columns, a 400 mm internal diameter column, and the CASTOR pilot plant itself. Figure 1 represents the 400 mm inner diameter column. This column operates at atmospheric pressure and room temperature. For pressure drop measurements, gas is air and liquid is water. The height of the packed bed is 1.5 m. The drip point density of the liquid distributor, dp , is 111 m⁻² for liquid loads between 8 m³/m²/h and 16 m³/m²/h, and 430 m⁻² for higher liquid loads. According to Fair and Bravo (1990), Aroonwilas *et al.* (2001) and Alix and Raynal (2008), it is high enough to ensure

that the distributor does not influence the results. Liquid load, Q_L , varies from 10 to 120 m³/m²/h. Superficial gas velocity, V_{SG} , varies from 0.5 to 4.2 m/s which leads to a F -Factor, F_s , varying from 0.5 to 4.6 Pa^{0.5}. The CASTOR pilot plant consists in a 1 100 mm internal diameter column. The pressure is close to the atmospheric pressure and the temperature varies from 40 to 70°C. Gas is flue gas. This CASTOR pilot plant was equipped with four packed beds, all of 4.25 m in height. The authors have observed that the bed density obtained with the 400 mm diameter column and the pilot plant are similar to each other and close to the one given for industrial plants by Koch Glitsch LP (IMTP Brochure, 2003). Q_L varies from 10 to 40 m³/m²/h, F_s varies from 0 to 2 Pa^{0.5}. dp is about 100 m⁻².

Linek *et al.* (2001) and Nakov *et al.* (2007) have determined mass transfer performances of random packings. Linek *et al.* (2001) measured interfacial area for the random packing Rauschert-Metall-Sattel-Rings (RMSR) 50, in particular. The interfacial area is measured by diluted CO₂ (1 vol% in air) into aqueous 1N NaOH solution. The absorption column was constructed of a perspex tube of 290 mm inner diameter packed to the height of 1.2 m (Linek *et al.*, 1984). Two liquid distributors were used: for lower liquid flow rates ($Q_L < 20$ m³/m²/h) a disk liquid distributor with 2 500 openings of 3 mm diam. per square meter and at higher liquid flow rates a liquid distributor with 630 openings per square meter. The temperature of both inlet streams was maintained at 20 ± 0.3°C. The absorption experiments were performed at liquid load from 1 to 120 m³/m²/h and at gas velocities corresponding to F_s values in the range from 0.6 to 3.0 Pa^{0.5}.

Nakov *et al.* (2007) investigated the effective area of two types of highly effective random metal packings such as Raschig Super-Ring (RSR) No. 1.5 and IMTP50. They used the CO₂ (1 vol% in air) in 1N NaOH system in a 470 mm internal diameter column with a packing height of 2.4 m. This solution was used as a model system by Kolev *et al.* (2006). Liquid loads, Q_L , were varied from 5 to 200 m³/m²/h. All investigations were carried out at a constant gas velocity, equal to 1 m/s ($F_s = 1.1$ Pa^{0.5}). The pressure drop of the packing is investigated by using a differential manometer, with an accuracy of 0.1 Pa. The liquid phase distributor has 923 drip points per m².

Seibert *et al.* (2005) have obtained mass transfer performances of random and structured packings. Experiments have been carried out with random packings IMTP25 and IMTP40; and structured packings Montz B1-250, Montz A3-500 and Montz B1-500, in a 430 mm internal diameter column. A packed height of approximately 3.3 m was used. The interfacial area is

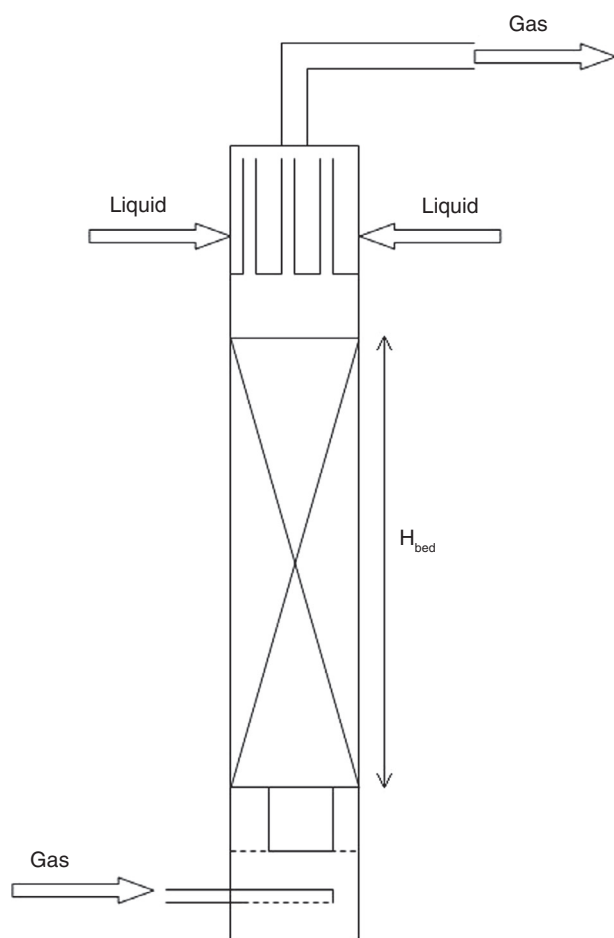


Figure 1

Sketch of the 400 mm inner diameter column.

measured by the air/0.1N NaOH absorption system. Liquid load, Q_L , was varied from 0 to 105 m³/m²/h. Superficial gas velocity, V_{SG} , is 1.5 m/s corresponding to a F -Factor, F_S , of 1.6 Pa^{0.5}.

Tsai *et al.* (2008, 2011) and Tsai (2010) have obtained hydrodynamics and mass transfer performances of structured packings. Authors measured pressure drops of structured packings, including Mellapak 125.Y, 2Y, 250.X, 250.Y and 500.Y. Authors also measured the mass transfer area of these structured packings, as a function of liquid load, surface tension, liquid viscosity, and gas rate. Tsai uses the same column and methods as Seibert. Gas velocity was varied from 0.6 to 2.3 m/s which corresponds to a F -Factor of 0.7 to 2.6 Pa^{0.5}.

To complete hydrodynamics data of structured packings, dry and wet pressure drop measurements for the structured packings Mellapak 125.X, 250.X, 250.Y and 500.Y presented by Spiegel and Meier (1992) are considered. Experiments were carried out with air/water at ambient conditions in a 1 m internal diameter column. Liquid load, Q_L , was varied from 0 to 200 m³/m²/h, superficial gas velocity, V_{SG} , from 0 to 7.5 m/s which leads to a F -Factor, F_S , varying from 0 to 8.3 Pa^{0.5}. No information is given about the bed height and about the liquid distributor. Spiegel and Meier (1994) present the capacity, pressure drop and holdup for the structured packings Mellapak 250.Y and 250.X measured at liquid loads up to 200 m³/m²/h. They discussed the pressure drop model presented in 1992 (Spiegel and Meier, 1992) with respect to its validity at high liquid loads and compare their model with other previous published work.

All these hydrodynamics and mass transfer data on random and structured packings will be compared with present ones.

2 EXPERIMENTAL TOOLS

2.1 Columns and Packings

For this work, experiments have been carried out in the same 400 mm internal diameter column than Alix and Raynal (2009). Olujic (1999) studied the effect of column diameter on pressure drop of a corrugated sheet structured packing. This author highlighted that the pressure drop increases and the capacity decreases when the column diameter decreases. This pressure drop increase and this capacity decrease become significant when the column diameter is close or equal to the height of a packing element. Thus, since the height of a packing element is close to 210 mm, it is considered that performing tests in the 400 mm internal diameter column ensure reliable results.

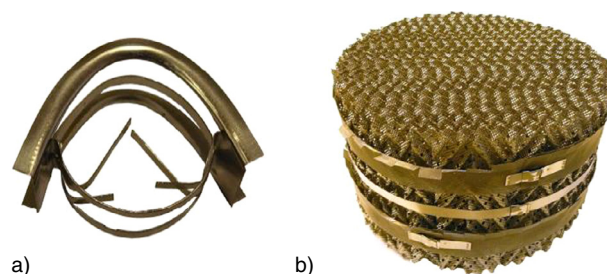


Figure 2

Pictures of packings tested: a) I-Ring#50 and b) Mellapak 350.X.

Both, random and structured packing types have been considered. Concerning random packings, experiments have been carried out with I-Ring#50, represented in Figure 2a. I-Ring#50 and IMTP50 are said to be identical, but we consider interesting to validate this. Geometric characteristics of these two random packings are given in Table 1. I-Ring#50 has been tested in the 400 mm inner diameter column with a bed height of 1.4 m. The density of the I-Ring#50 packed bed in the 400 mm internal diameter column is similar to the density of the IMTP50 packed bed tested by Alix and Raynal (2009) in the same column.

It has to be underlined that the column diameter to the characteristic length of the IMTP50 ratio is close to 8. This is the minimum value according to De Brito *et al.* (1994), however Alix and Raynal (2009) showed that it is large enough since packed bed density and pressure drop are similar to those measured in the CASTOR pilot plant ($D = 1100$ mm) where this ratio is much higher and close to 20.

Concerning the structured packing, the Mellapak 350.X (Sulzer Chemtech), represented in Figure 2b, has been tested in the 400 mm inner diameter column with a bed height of 1.1 m. This packing has been chosen to test a more efficient packing. Geometric characteristics of this structured packing are given in Table 2.

2.2 Pressure Drop Measurements

Hydrodynamic characterization of the random packings I-Ring#50, IMTP50 (Alix and Raynal, 2009) and of the structured packing Mellapak 350.X has consisted in measuring pressure drop in the column for different liquid loads and different F -Factor. Repeatability measurements have been performed for some liquid loads and F -Factor.

Pressure drop is measured between the inlet and the outlet of the bed with either two inclined or two horizontal tubes. It has been checked that, if one uses the same pressure tap geometry for both sampling ports, this geometry does not influence the results. Note that the lines of the transducer are purged before each measurement. For wetted conditions, pressure drop fluctuates in time, present values are thus time averaged over a period of 2 minutes. Relative error is estimated between 10 and 20%. The packed bed is not pre-wetted *via* a high liquid flowrate.

Dry pressure drop curves in function of F -Factor have also been determined. Column pressure, temperature at the head of the column and gas temperature at the inlet have been measured to determine gas density. These measurements allowed to determine wetted pressure drop curves in function of F_s . The flooding limit for each liquid mass flow rate corresponds to the F -Factor from which pressure drop increases drastically.

2.3 Interfacial Area Measurements

Different chemical systems have been used to performed interfacial area measurements in the 400 mm internal diameter columns. [Alix and Raynal \(2009\)](#) used two CO_2/NaOH systems to performed interfacial area measurements with IMTP50: NaOH at 1N with air as used by [Duss et al. \(2001\)](#) and NaOH at 0.1N with air as used by [Seibert et al. \(2005\)](#). They found that the interfacial area is systematically 10% higher with the air-0.1N than the one measured with the air-1N system. This difference between these two systems can be explained by a gas limitation. Thus, for I-Ring#50 and Mellapak 350.X, interfacial area measurements have been performed with NaOH at 0.1N with air. In all these cases, a pseudo-first order reaction, a fast reaction regime and a negligible gas side resistance are assumed. This leads to the following equation ([Danckwerts, 1970](#)):

$$\phi_{\text{CO}_2} = \frac{E \cdot k_L}{He} \cdot P_{\text{CO}_2} \cdot a_e = \frac{\sqrt{D_{\text{CO}_2} \cdot k_2 \cdot C_{\text{OH}}^0}}{He} \cdot P_{\text{CO}_2} \cdot a_e \quad (1)$$

ϕ_{CO_2} is the absorption rate of CO_2 . E , is the enhancement factor and takes into account the effect of the chemical reaction on ϕ_{CO_2} . k_L is the liquid side mass transfer coefficient. P_{CO_2} , is the partial pressure of CO_2 . Kinetic constant, k_2 , CO_2 liquid diffusion coefficient, D_{CO_2} , and Henry constant, He , have been calculated with equations given by [Pohorecki and Moniuk \(1988\)](#).

Within the packed column, one dimensional and stationary plug flows of liquid and gas are assumed. The column is assumed to be isotherm and isobar. The CO_2

gas molar fraction is measured at the inlet and at the outlet of the column *via* infra-red apparatus. From previous studies on liquid distribution ([Alix and Raynal, 2008](#)), liquid flow is considered homogeneous in particular due to the fact that a high drip points density distributor is used. Thus, the effective area, a_e , is assumed to be constant all along the column. From the inlet CO_2 molar fraction, $y_{\text{CO}_2, \text{in}}$, a_e is the only parameter to adjust in order to fit the CO_2 outlet molar fraction. Then, from the CO_2 profile one directly gets a_e . Liquid samples are taken at the inlet and outlet of the column to measure. CO_3^{2-} and OH^- amounts by HCl titration. The concentration of OH^- in the liquid bulk, C_{OH}^0 , can be implemented into the 1D model.

3 RESULTS

3.1 Random Packings

3.1.1 Hydrodynamics

[Figure 3](#) shows dry pressure drop experimental data of I-Ring#40, I-Ring#50, IMTP50 and I-Ring#70 *versus* F -Factor. [Figure 4](#) presents measured wetted pressure drop of the same packings *versus* F -Factor for a liquid load around $30\text{--}35 \text{ m}^3/\text{m}^2/\text{h}$. Sulcol simulations (3.0.8) are also presented for I-Ring#50. For a fixed gas/liquid contactor and a fixed liquid load, pressure drop increases with the F -Factor. At 400 mm and 1 000 mm, the slope of the curve equals 2 which is comparable to a gas turbulent flow in pipes. [Figures 3 and 4](#) show that I-Ring#50 (present work and [Kehrer et al., 2006](#)) and IMTP50 pressure drop are similar in a range of $\pm 30\%$, which is higher

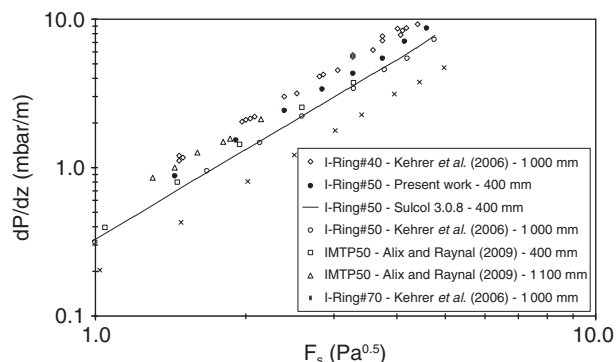


Figure 3

Experimental dry pressure drop data *versus* F -Factor for I-Ring#40, I-Ring#50, IMTP50 and I-Ring#70.

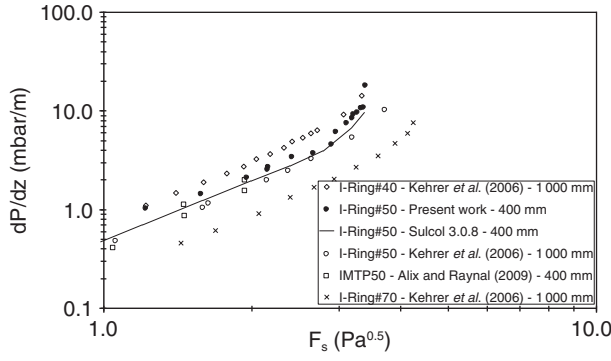


Figure 4
Experimental wetted pressure drop data versus F -Factor for I-Ring#40, I-Ring#50, IMTP50 and I-Ring#70 at $Q_L = 30\text{-}35 \text{ m}^3/\text{m}^2/\text{h}$.

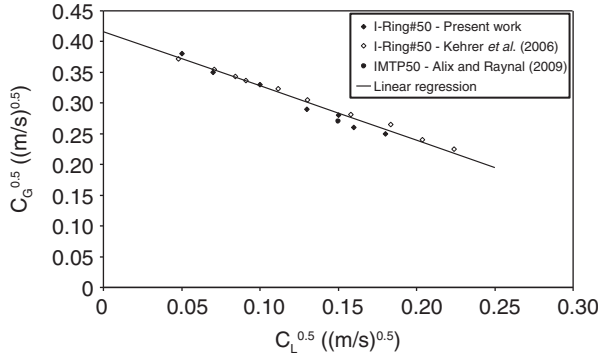


Figure 5
Wallis diagram of I-Ring#50 and IMTP50 packings and best linear fit.

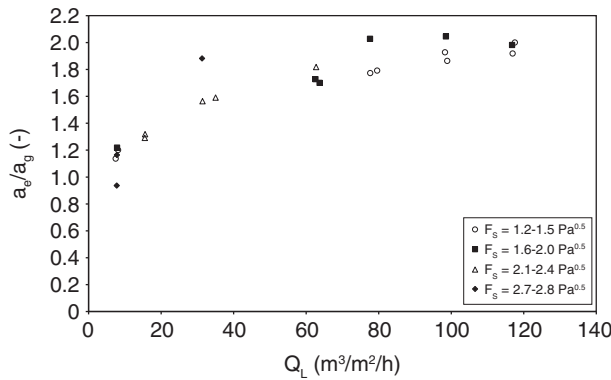


Figure 6
Normalized interfacial area as a function of Q_L for I-Ring#50. Influence of the F -Factor.

than the experimental uncertainty of $\pm 10\text{-}20\%$. Then, there is a small scale effect between 400 and 1 000 mm diameter columns: this is in agreement with Olujic (1999), which has highlighted a difference of 30% between pressure drop obtained in a 450 mm inner diameter column and those obtained in a 800 mm inner diameter column for a liquid load of $10 \text{ m}^2/\text{m}^3/\text{h}$. Note that pressure drop values increase and that the flooding limit decreases when the geometric area increases. Present data show that I-Ring#50 has a flooding limit 10% lower than those of Kehrler's data; this slight difference can be explained by the column diameter influence and/or the experimental uncertainty.

Figure 5 represents the capacity in a Wallis diagram (Wallis, 1969) for packing I-Ring#50 and IMTP50. The gas capacity factor, C_G , has been determined from the flooding limit measurement. In this Wallis diagram, the square root of this gas capacity factor is represented as a function of the square root of the liquid capacity factor, C_L , respectively given by Equations (2) and (3):

$$C_G = V_{SG} \left(\frac{\rho_G}{\rho_L - \rho_G} \right)^{0.5} \quad (2)$$

$$C_L = V_{SL} \left(\frac{\rho_L}{\rho_L - \rho_G} \right)^{0.5} \quad (3)$$

where V_{SL} is the superficial liquid velocity and the liquid density.

I-Ring#50 measurements of present work are in agreement with those of Kehrler et al. (2006). Although only one data is available for IMTP 50, it is in agreement with the I-Ring#50 data. All these data are well represented by the following linear regression:

$$C_G^{0.5} = -0.8854 \times C_L^{0.5} + 0.4161 \quad (4)$$

3.1.2 Mass Transfer

Figure 6 represents the present I-Ring#50 normalized interfacial area measurements versus the liquid load for different F -Factors. This figure shows that the I-Ring#50 normalized interfacial area measurements increase with the liquid load from 1 to 2. Note that the measurement performed at $31 \text{ m}^3/\text{m}^2/\text{h}$ at $F_S = 2.7\text{-}2.8 \text{ Pa}^{0.5}$ corresponds to a capacity factor, F_C , of 80%, that is why this measurement is higher than all the others. At a constant liquid load the F -Factor does not influence the normalized interfacial area significantly: the dispersion of the data is of the order of $\pm 10\%$.

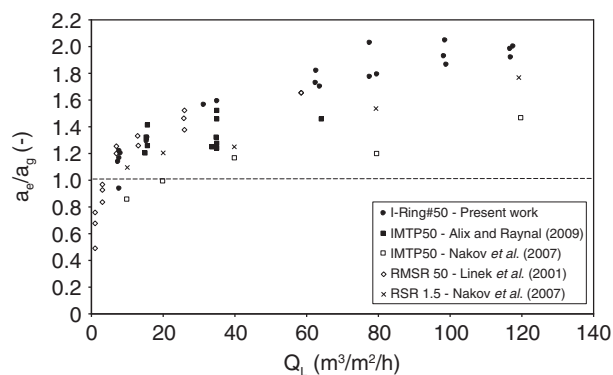


Figure 7

Normalized effective area as a function of Q_L , for the I-Ring#50. Comparison with other similar random packings. $F_S = 1-3 \text{ Pa}^{0.5}$.

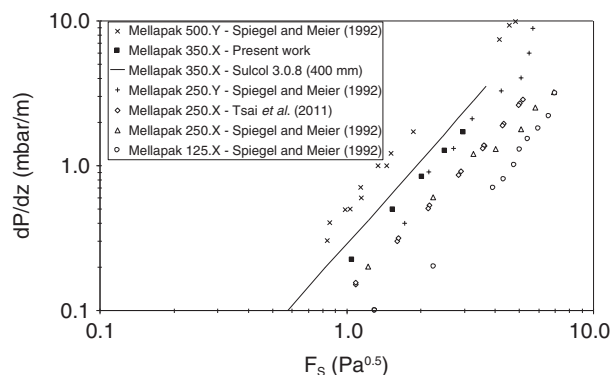


Figure 8

Dry pressure drop experimental data of Mellapak structure packings versus F -Factor.

Normalized interfacial areas of random packings similar to the I-Ring#50 are presented as a function of Q_L for a F -Factor of $1-3 \text{ Pa}^{0.5}$ in Figure 7. It was expected to obtain similar interfacial areas between I-Ring#50 and IMTP50 since these packings have identical geometric characteristics (Tab. 1). Although data have been obtained in different internal diameter columns and with different chemical systems, they are coherent with each other. The four packings present interfacial areas higher than their geometrical area when Q_L is above about $10 \text{ m}^3/\text{m}^2/\text{h}$. This result is in agreement what is observed by Seibert *et al.* (2005) for the IMTP40 packing. One observes a gap between ratios of IMTP50 measured by Alix and Raynal (2009) and ratios measured by Nakov *et al.* (2007). Although these data have been obtained

for similar F -Factor, two different chemical systems have been used. Actually, Alix and Raynal (2009) have pointed out that the use of the chemical system 1N could lead to 10% lower interfacial area than the use of 0.1N. Moreover, Nakov *et al.* (2007) used different kinetic and thermodynamic models. These differences could explain the trend observed on the IMTP50 ratios. The normalized interfacial areas measured on the I-Ring#50 are in good agreement with those obtained by Linek *et al.* (2001) with RMSR 50. However, they are higher than those obtained by Nakov *et al.* (2007) with RSR 1.5. This difference can be explained by the use of different kinetic and different thermodynamic models. Thus, the ratios of I-Ring#50 seem equivalent, and sometimes higher, than those of the other packings. To conclude, it should be noted, first, that there is a good agreement between normalized interfacial areas of random packings similar to the I-Ring#50 and, second, that these normalized interfacial areas are between 1 and 2 for $Q_L > 10 \text{ m}^3/\text{m}^2/\text{h}$.

3.2 Structured Packings

3.2.1 Hydrodynamics

Figure 8 represents dry pressure drop experimental data of Mellapak structured packings: Mellapak 500.Y, Mellapak 350.X, Mellapak 250.Y, Mellapak 250.X and Mellapak 125.X. Experimental data of Mellapak 350.X are compared with Sulcol 3.0.8 simulations. At 400 and 1 000 mm and for the three packings, the slope of the curve equals 2 which is comparable to a turbulent gas flow in pipes, as for the random packings. Besides, our experimental pressure drop data are in coherence with data from Spiegel and Meier (1992) and Tsai *et al.* (2011) showing a pressure drop decrease with a decrease in packing geometric area. Mellapak 350.X and Mellapak 250.Y present similar dry pressure drop. Note that, for a F -Factor higher than $4 \text{ Pa}^{0.5}$, a slight shift is observed between Mellapak 250.X pressure drop obtained in a 400 mm internal diameter column and those obtained in a 1 000 mm internal diameter column. It is observed that dry pressure drop data of the Mellapak 350.X are 20% lower than predicted by Sulcol 3.0.8 for the same diameter.

Figure 9 represents wetted pressure drop experimental data of Mellapak 350.X versus F -Factor for a liquid load of $31 \text{ m}^3/\text{m}^2/\text{h}$. They are compared with Sulcol 3.0.8 simulations in a 400 mm internal diameter column. There is a relative good agreement between experimental data and Sulcol 3.0.8 simulations. However, the experimental flooding point is 20% lower than predicted by the manufacturer software. This early flooding may be due to the type of wall wipers on the packing or experimental uncertainty of flooding ($\pm 20\%$).

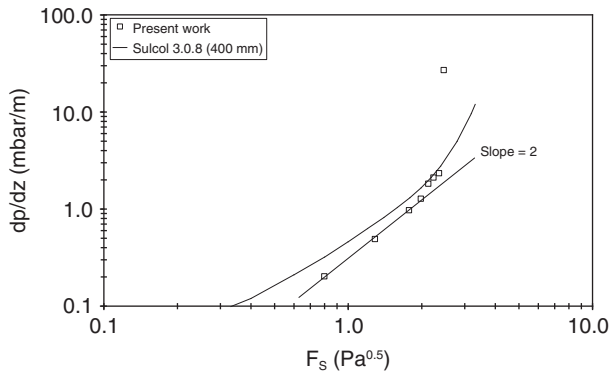


Figure 9

Wetted pressure drop experimental data of Mellapak 350.X versus F -Factor for a liquid load of $31 \text{ m}^3/\text{m}^2/\text{h}$. Comparison with Sulcol 3.0.8 simulations.

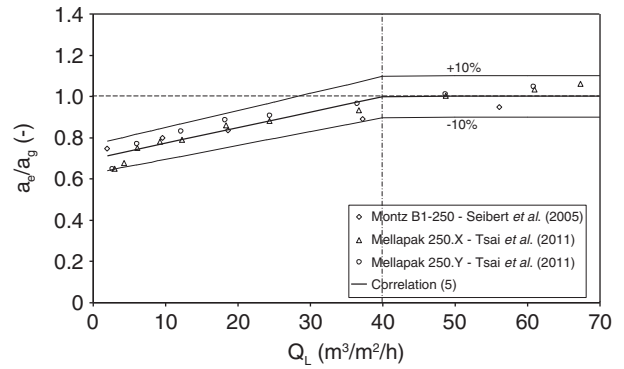


Figure 11

Normalized interfacial area as a function of Q_L for 250 series structured packings. $F_S = 0.7\text{-}2.6 \text{ Pa}^{0.5}$.

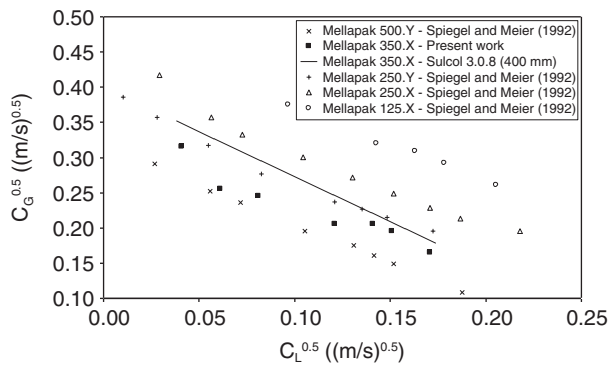


Figure 10

Wallis diagram capacity of Mellapak structured packings.

Figure 10 represents the capacity of the different Mellapak structured packings in a Wallis diagram. Experimental data of Mellapak 350.X are compared with Sulcol 3.0.8 simulations. As expected the capacity of the packing increases with the decrease of the geometric area. From this figure, one deduces that the Mellapak 125.X is at least 30% more capacitive than the Mellapak 250.X, 50% more than the Mellapak 250.Y, 60% more than the Mellapak 350.X and finally 90% more capacitive than the Mellapak 500.Y. There is a good agreement between experimental data and Sulcol 3.0.8 simulations, experimental data are less than 20% lower.

3.2.2 Mass Transfer

Figure 11 represents the normalized interfacial area as a function of Q_L for 250 series structured packings. For each liquid load data represented corresponds to an

average value for the whole range of F_S studied, this average is justified since almost no gas influence has been observed on the interfacial area for a constant liquid load.

Tsai *et al.* (2011) have noticed that the mass transfer area was most strongly related to specific area and liquid load; on the contrary, it was little dependent on the gas velocity, the surface tension or the liquid viscosity the latter being varied on the respective range of 30-72 mN/m and 1-15 mPa.s. Then, for the present study, physical properties impact has been neglected. For all packings, the normalized interfacial area increases with the liquid load, and tends to reach 1 for a sufficiently high liquid load. Then a_g could be considered as the effective area for structured packings above a certain liquid load. Thus, the following correlation (5) is proposed to predict the normalized interfacial area of structured packings of $250 \text{ m}^2/\text{m}^3$ geometric area, with an uncertainty of $\pm 10\%$:

$$\begin{cases} \text{for } 2 \leq Q_L < 40 \text{ m}^3/\text{m}^2/\text{h}, & a_e/a_g = 0.0075 \times Q_L + 0.697 \\ \text{for } Q_L \geq 40 \text{ m}^3/\text{m}^2/\text{h}, & a_e/a_g = 1 \end{cases} \quad (5)$$

Figure 12 represents the normalized area as a function of Q_L for structured packings with geometric area in the range of $350\text{-}500 \text{ m}^2/\text{m}^3$. For the Mellapak 350.X, the normalized interfacial area increases with the liquid load and tends to reach 1 for a sufficiently high liquid load, like the 250 series structured packings (Fig. 11). Although the normalized interfacial area of the Montz B1-500 packing has not been measured for liquid loads higher than $30 \text{ m}^3/\text{m}^2/\text{h}$, the same trend as observed for the Mellapak 350.X is followed. Concerning the Montz A3-500, the

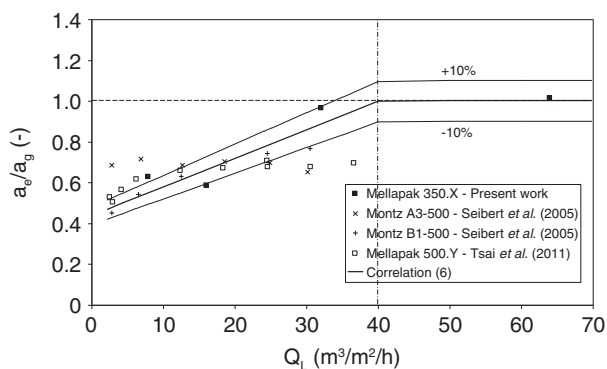


Figure 12

Normalized interfacial area as a function of Q_L for structured packings with a geometric area of 350-500 m^2/m^3 . $F_S = 0.5\text{-}2.3 \text{ Pa}^{0.5}$.

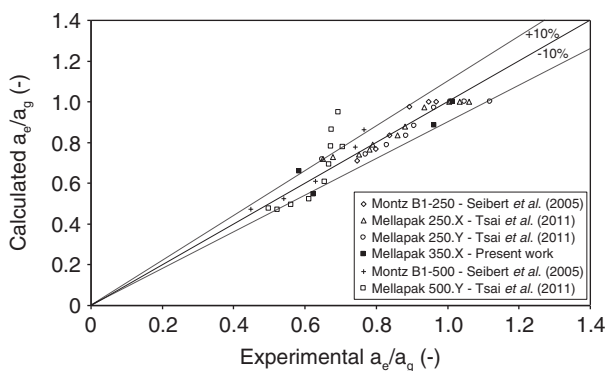


Figure 13

Comparison of measured and calculated values of normalized interfacial area from correlations (5) and (6).

normalized interfacial area is nearly constant, which can be interesting at low liquid loads. However, the behaviour of the Montz A3-500 packing is very different of those of the Montz B1-500 and the Mellapak 350.X packings. This can be explained by the difference in material: the Montz A3 is a special wire mesh packing whereas the Montz B1-500 and the Mellapak 350.X are metal sheet packings. Since the Montz A3-500 packing presents a very different behaviour of metal sheet packings, only metal sheet packings are considered in the following. The following correlation is proposed to predict, with an uncertainty of $\pm 10\%$, the normalized interfacial area of structured packings with a geometric area of 350-500 m^2/m^3 :

$$\begin{cases} \text{for } 2 \leq Q_L < 40 \text{ m}^3/\text{m}^2/\text{h}, & a_e/a_g = 0.014 \times Q_L + 0.4368 \\ \text{for } Q_L \geq 40 \text{ m}^3/\text{m}^2/\text{h}, & a_e/a_g = 1 \end{cases} \quad (6)$$

when comparing Equations (5) and (6), it can be first noted that at higher geometric area, one requires a higher liquid load to take fully advantage of the packing. Indeed, for low liquid loads, high geometric area packings developed an interfacial area equal to about 50% of their geometric area, while low geometric area packings developed an interfacial area equal to about 70% of their geometric area. This behaviour can be explained by a wettability issue. Second, one observes that for all packings, the same liquid load value of 40 $\text{m}^3/\text{m}^2/\text{h}$ is the minimum value to ensure a a_e/a_g ratio equal to 1.

Figure 13 compares the measured and calculated values of normalized interfacial areas from correlations (5) and (6). A good agreement of $\pm 10\%$ between the experimentations and the correlations is observed. No general correlation is proposed for random packings since a_e/a_g ratio is strongly linked to their geometrical area (Wilson, 2004). To illustrate this, IMTP50 can strongly exceed a_g while IMTP15 tends to reach a_g .

4 DISCUSSION

The choice of a packing depends on its capacity, and associated pressure drop, and its interfacial area. These characteristics are respectively required to determine the column diameter and the column height. In the following, structured and random packings are then first compared in terms of capacity for two range of geometric area. Second, they are compared in terms of interfacial area, and finally in terms of coupling hydrodynamics and mass transfer.

4.1 Hydrodynamics

The purpose of Figure 14 is to compare capacity of structured and random packings for the range of geometric area: 60-150 m^2/m^3 in a Wallis representation. This figure shows clearly that structured packings are more capacitive (25-30%) than random packings for similar geometric area. This could be explained by at least two reasons. First, a non negligible amount of droplets is generated with such random packings (Alix and Raynal, 2009). Second, structured packings generate lower void fractions for given geometric areas.

Figure 15 represents in a Wallis diagram the capacity of different packings for the range of geometric area 230-350 m^2/m^3 . This figure shows clearly that all structured packings are more capacitive than the two random packings (I-Ring#15 and I-Ring#25).

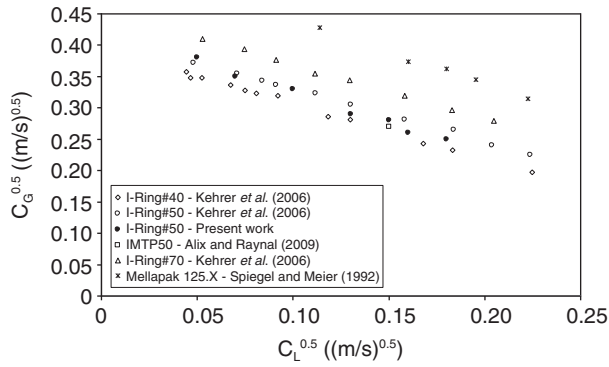


Figure 14
Wallis diagram for different packings with a similar geometric area ($60\text{-}150\text{ m}^2/\text{m}^3$).

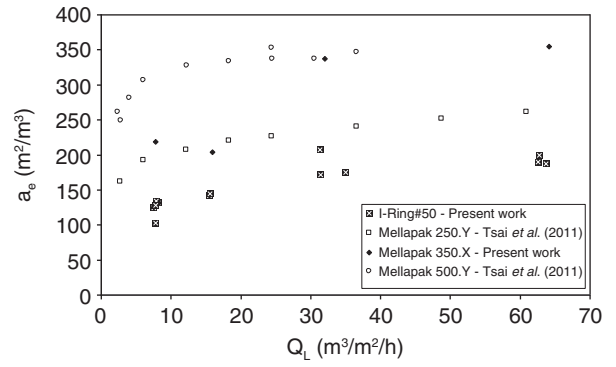


Figure 16
Interfacial area as given by relation (1) as a function of Q_L , for different structured and random packings.

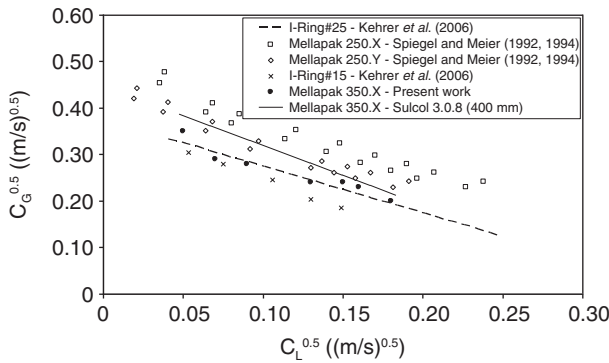


Figure 15
Wallis diagram for different packings with a similar geometric area ($230\text{-}350\text{ m}^2/\text{m}^3$).

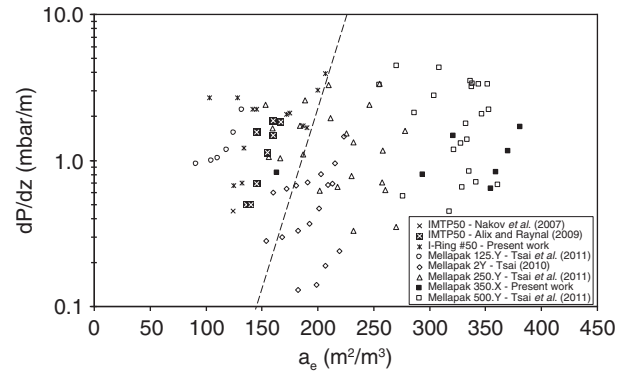


Figure 17
Comparison of the pressure drop of structured packings with pressure drop of random packings.

4.2 Coupling Hydrodynamics and Mass Transfer

Figure 16 represents interfacial area as given by relation (1) as a function of Q_L , for different structured and random packings. It has to be underlined that the capacity of such packings is comparable (Fig. 12, 14). Figure 16 shows that, in spite of the fact that random packings could lead to higher a_e/a_g , structured packings generate higher absolute values of effective areas, the geometric geometry for comparable capacity being much higher.

Figure 17 compares pressure drop of structured packings with pressure drop of random packings as a function of interfacial area. It has to be noticed that last generation random packings, like RSR (Chambers and Schultes, 2006), have not been considered for this study. This is explained by the fact that there is a lack of data concerning both capacity and a_e for such packings. Then, present conclusions should be updated

when enough data will be available. In Figure 17, liquid loads are limited to $70\text{ m}^3/\text{m}^2/\text{h}$ to correspond to the range expected in CO_2 post-combustion capture, and gas flowrates are between 30 and 80% of flooding. For the following structured packings, Mellapak 125.Y, 250.Y and 500.Y, interfacial areas correspond to experimental measurements while pressure drop data are simulated with Sulcol 3.0.8 for F -Factor between 0.7 and 2.6 $\text{Pa}^{0.5}$. Indeed, since Tsai et al. (2011) only give a range of F -Factor for which interfacial areas have been measured, it is difficult to determine precisely at which interfacial area corresponds which pressure drop. In Figure 17, all random packings considered develop an interfacial area less than $207\text{ m}^2/\text{m}^3$ for corresponding pressure drop between 0.3 and 4 mbar/m. Among structured packings, only Mellapak 125.Y has similar characteristics. All other structured packings present similar pressure drop but

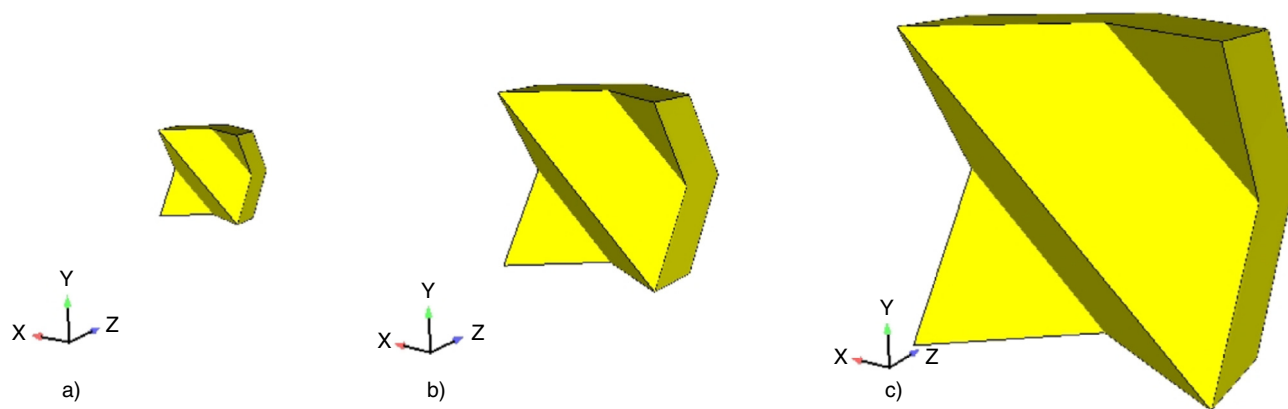


Figure 18

CFD simulations – Representative periodic element unit (REU) illustration a) Mellapak 500.Y, b) Mellapak 250.Y, c) Mellapak 125.Y.

offer higher interfacial areas. As can be seen in [Figure 17](#), all latter packings are on the right hand side of the line which symbolizes the limit between the performances of the random packings (on the left-hand side) and the structured packings. With structured packings, one reaches up to $220 \text{ m}^2/\text{m}^3$, $280 \text{ m}^2/\text{m}^3$, $380 \text{ m}^2/\text{m}^3$ and $360 \text{ m}^2/\text{m}^3$, respectively, for 2Y, 250.Y, 350.X and 500.Y. Thus, structured packings meet the target of both low pressure drop and high interfacial area as required for post-combustion carbon capture. From [Figure 17](#), one deduces that the best packings, in terms of a compromise between pressure drop and interfacial areas, are Mellapak 350.X and 500.Y. Only a techno-economical evaluation based on the correlation presented in the present paper ([Eq. 5, 6](#)) can determine which one is the most appropriate packing for the CO_2 post-combustion capture.

5 CFD MODELING FOR FUTURE GEOMETRIES

The previous section has highlighted that structured packings are more interesting than random packings in terms of hydrodynamics and mass transfer performances for post-combustion carbon capture. Recently, optimized structured packings such as MCC ([Menon and Duss, 2011](#)) or 4D ([Alix et al., 2011](#)) have been proposed. As the developments of such packings are time consuming, it is of high interest to develop a screening methodology which could be used to predict the performances of novel geometries. It is discussed in the following how CFD could be used in this objective.

It has been shown that interfacial area of structured packings corresponds to their geometric area above a liquid load of $40 \text{ m}^3/\text{m}^2/\text{h}$ ([Eq. 5, 6](#)) and that the capacity is a function of dry pressure drop. As the interfacial

area predicts the geometric area, the main challenge is, thus, to predict dry pressure drop in structured packings. In this context, CFD can be an interesting tool in complement of experimental works to investigate performance characteristics of structured packings. Indeed, CFD is more and more used to calculate flow characteristics in packed beds. In recent years, several works have been published in the literature, which deal with the CFD simulations in structured packings ([Petre et al., 2003](#); [Raynal et al., 2004](#); [Ataki, 2006](#); [Raynal and Royon-Lebeaud, 2007](#); [Haroun et al., 2010a,b, 2012](#)). These works show that CFD can be an interesting tool in addition to experimental works to determine local hydrodynamics parameters as pressure drop, liquid holdup, wetting quality, and mass transfer coefficients.

In this work, dry pressure drop determination in structured packings by CFD is investigated. In this purpose three dimensional simulations have been carried out considering a computational domain which corresponds to the smaller periodic Representative Elementary Unit (REU) of structured packing Mellapak: 125.Y, 250.Y and 500.Y. [Figure 18](#) shows the REU simulation domain for each configuration. The computational method is based on Large Eddy Simulations (LES). This CFD approach solves explicitly the large turbulent scales and modeling assumptions are restricted to small scales only. The sub grid model used is based on the WALE model formulation. The assumptions of this model remain the same than in Smagorinsky model but involve local rotation rate in the expression of the turbulent viscosity; this is justified since dissipative scales are also characterized by high rotation rate. The WALE model thus allows to predict the correct wall behaviour with implicit damping effect. Present LES differs from previous calculations performed by [Petre et al. \(2003\)](#)

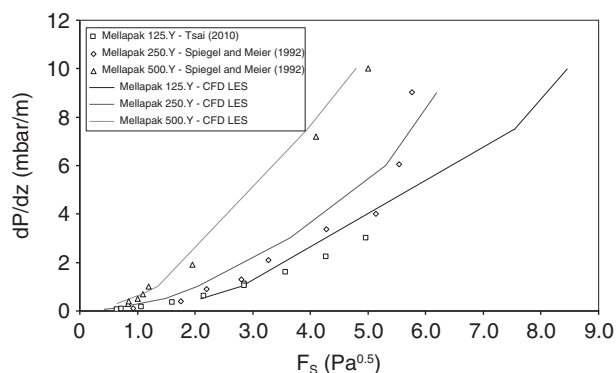


Figure 19

CFD simulations – Comparison with experimental dry pressure drop data.

or Raynal *et al.* (2004) who used more standard models (RANS k - ϵ or laminar models) and is thus much more demanding in terms of mesh, solver, boundary conditions definition and CPU time.

Simulations are carried out with the commercial CFD software Ansys Fluent 12. Second order implicit scheme was chosen for time transition formulation. For pressure interpolation, second order scheme is adopted and SIMPLEC for pressure-velocity coupling. For solving momentum equation a bounded central differencing discretization scheme is used.

CFD present results are shown in Figure 19 where they are compared with experimental data of Spiegel and Meier (1992). The results show that the LES approach is well adapted to predict dry pressure drop in structured packings. Indeed, the comparison between simulated and experimental dry pressure drop, for different gas F -factor shows that simulated dry pressure are in good agreement with experimental data of Spiegel and Meier (1992). The relative error between LES simulations results and experimental data is about 10% for a large range of gas flow rates. As it has been shown before that the more capacitive is the packing, the less is the dry pressure drop; it makes sense to simulate dry pressure drop data. Present simulations show that the CFD can be used as an effective tool to perform preliminary tests of new and original geometries or to benchmark between different existing packing technologies.

In a close future, such approach will be also be used for calculations for X geometries.

CONCLUSION

Structured and random packings are commonly considered for post-combustion CO₂ capture processes. In this study, hydrodynamics and mass transfer performances

of these two types of packings are discussed in terms of pressure drop, capacity and mass transfer parameters, in order to determine which type of packings is the most appropriate for post-combustion CO₂ capture. To complete the data available in the literature, experiments have been carried out with the I-Ring#50 random packing and the Mellapak 350.X structured packing. Concerning random packings, it has been shown that I-Ring#50 hydrodynamics is similar to those of the IMTP50. A linear regression has been proposed to predict the capacity of these random packings in a Wallis representation. The evolution of the normalized interfacial area of the I-Ring#50 is coherent with those of other similar random packings. Concerning structured packings, Mellapak 350.X hydrodynamics is in agreement with trends observed by other authors with other Mellapak packings. Normalized interfacial area of Mellapak 350.X tends to reach 1 for a sufficiently high liquid load like other structured packings. Two correlations have been proposed to predict with $\pm 10\%$ of uncertainty the normalized interfacial area of metal sheet structured packings: one for the 250 series structured packings and one for the 350-500 m²/m³ geometric area structured packings. It is observed that for liquid load above 40 m³/m²/h, the effective area for structured packings is equal to their geometric area. This behaviour is different of those of random packings, which could lead to normalized interfacial area up to 2. The comparison of the capacity of structured and random packings has highlighted that structured packings are both more capacitive and develop higher interfacial areas. Thus, structured packings are more appropriate than random packings for post-combustion CO₂ capture processes.

It is discussed how CFD can be used as an effective tool to perform preliminary tests of original geometries or to benchmark different existing packing technologies. One can easily determine a first estimation of pressure drop and interfacial areas which could be further used in techno-economic studies which would confirm or not the interest of the tested geometries.

REFERENCES

- Alix P., Raynal L. (2008) Liquid Distribution and Liquid Hold-up in Modern High Capacity Packings, *Chem. Eng. Res. Des.* **86**, 585-591.
- Alix P., Raynal L. (2009) Pressure Drop and Mass Transfer of a High Capacity Random Packing. Application to CO₂ Post-combustion Capture, *Energy Procedia* **1**, 845-852.
- Alix P., Raynal L., Abbe F., Meyer M., Prevost M., Rouzineau D. (2011) Mass transfer and hydrodynamic characteristics of new carbon carbon packing: Application to CO₂ post-combustion capture, *Chem. Eng. Res. Des.* **89**, 1658-1668.

- Aroonwilas A., Tontiwachwuthikul P., Chakma A. (2001) Effects of operating and design parameters on CO₂ absorption in columns with structured packings, *Sep. Purif. Technol.* **24**, 403-411.
- Ataki A. (2006) Wetting of Structured Packing Elements – CFD and Experiment, *PhD Thesis*, Technical University of Kaiserslautern.
- Chambers S., Schultes M. (2006) How to surpass conventional and high capacity structured packings with Raschig Super-Pak, *Distillation and Absorption conference*, 4-6 Sept., London, 241-251.
- Danckwerts P.V. (1970) *Gas-Liquid Reactions*, McGraw-Hill, New-York.
- De Brito M.H., Von Stockar U., Bangester A.M., Bomio P., Laso M. (1994) Effective mass transfer area in a pilot plant column equipped with structured packing and with ceramic rings, *Ind. Eng. Chem. Res.* **33**, 647-656.
- Duss M., Meierhofer H., Dale E. (2001) Effective Interfacial area and liquid holdup of nutter rings at high liquid loads, *Chem. Eng. Technol.* **24**, 716-723.
- Fair J.R., Bravo J.L. (1990) Distillation columns containing structured packing, *Chem. Eng. Prog.* **86**, 19-29.
- Feron P.H.M., Abu-Zahra M., Alix P., Biede O., Broutin P., de Jong H., Kittel J., Knudsen J., Raynal L., Vilhelmsen P.J. (2007) *3rd International Conference on Clean Coal Technologies for our Future*, Caligari, Italy.
- Haroun Y., Legendre D., Raynal L. (2010a) Direct numerical simulation of reactive absorption in gas-liquid flow on structured packing using interface capturing method, *Chem. Eng. Sci.* **65**, 351-356.
- Haroun Y., Legendre D., Raynal L. (2010b) Volume of fluid method for interfacial reactive mass transfer: application to stable liquid film, *Chem. Eng. Sci.* **65**, 2896-2909.
- Haroun Y., Raynal L., Legendre D. (2012) Mass transfer and liquid hold-up determination in structured packing by CFD, *Chem. Eng. Sci.* **75**, 342-348.
- IMTP Brochure (2003) Bulletin KGIMTP-I 2M0303B. Available at http://www.koch-glitsch.com/masstransfer/pages/IMTP_metal.aspx.
- Kehrer F., Spiegel L., Kolesnikov E., Choo P. (2006) Experimental investigation and modelling of Sulzer I-Ring hydraulics, *Chem. Eng. Res. Des.* **84**, 1075-1080.
- Knudsen J.N., Vilhelmsen P.J., Jensen J.N., Biede O. (2006) *VGB Conference, Chemie in Kraftwerk*, Germany, 11-12 Oct.
- Knudsen J.N. (2009) *European Conference on CCS research*, 10-11 Feb., Oslo, Norway.
- Kolev N., Nakov S.V., Ljutzkanov L., Kolev D. (2006) Effective Area of a Highly Effective Random Packing, *Chem. Eng. Process.: Process Intensification* **45**, 429-436.
- Linek V., Petricek P., Benes P., Brun R. (1984) Effective interfacial area and liquid side mass-transfer coefficients in absorption columns packed with hydrophilized and untreated plastic packings, *Trans. IChemE, Part A, Chem. Eng. Res. Des.* **62**, 13.
- Linek V., Moucha T., Rejl F.J. (2001) Hydraulic and mass transfer characteristics of packings for absorption and distillation columns. Rauschert-Metall-Sattel-Rings, *Trans. IChemE* **79**, 725-732.
- Menon A., Duss M. (2011) Sulzer – reducing the energy penalty for post-combustion CO₂ capture, *Carbon Capture J.* Sept-Oct, 2-5.
- Nakov S.V., Kolev N., Ljutzkanov L., Kolev D. (2007) Comparison of the effective area of some highly effective packings, *Chem. Eng. Process.: Process Intensification* **46**, 1385-1390.
- Olujic Z. (1999) Effect of Column Diameter on Pressure Drop of a Corrugated Sheet Structured Packing, *Chem. Eng. Res. Des.* **77**, 505-510.
- Petre C.F., Larachi F., Illiuta I., Grandjean B.P.A. (2003) Pressure drop through structured packings: breakdown into the contributing mechanisms by CFD modeling, *Chem. Eng. Sci.* **58**, 163-177.
- Pohorecki R., Moniuk W. (1988) Kinetics of reaction between carbon dioxide and hydroxylions in aqueous electrolyte solutions, *Chem. Eng. Sci.* **43**, 1677-1684.
- Raynal L., Royon-Lebeaud A. (2007) A multi-scale approach for CFD calculations of gas-liquid flow within large size column equipped with structured packing, *Chem. Eng. Sci.* **62**, 7196-7204.
- Raynal L., Boyer C., Ballaguet J.P. (2004) Liquid hold-up and pressure drop determination in structured packing with CFD simulation, *Can. J. Chem. Eng.* **82**, 871-879.
- Raynal L., Gomez A., Caillat B., Haroun Y. (2013) CO₂ Capture Cost Reduction: use of a Multiscale Simulations Strategy for a Multiscale Issue, *Oil Gas Sci. Technol.* DOI: 10.2516/ogst/2012104.
- Seibert F., Wilson I., Lewis C., Rochelle G. (2005) Effective Gas/Liquid Contact Area of Packing for CO₂ absorption/stripping, *Greenhouse Gas Control Technol.* **2**, 1925-1928.
- Spiegel L., Meier W. (1992) A generalized pressure drop model for structured packings, *Distillation and Absorption, IChemE Symp. Series n° 128*, B85-B94.
- Spiegel L., Meier W. (1994) Capacity and pressure drop of structured packings at very high liquid loads, *AIChE 1994 Spring National Meeting*, 17-21 April.
- Tsai R.E. (2010) Mass Transfer Area of Structured Packing, *PhD Thesis*, University of Texas, Austin.
- Tsai R.E., Schultheiss P., Kettner A., Lewis J.C., Seibert A.F., Eldridge R.B., Rochelle G.T. (2008) Influence of Surface Tension on Effective Packing Area, *Ind. Eng. Chem. Res.* **47**, 1253-1260.
- Tsai R.E., Seibert A.F., Eldridge R.B., Rochelle G.T. (2011) A Dimensionless Model for Predicting the Mass-Transfer Area of Structured packing, *AIChE J.* **57**, 1173-1184.
- Wallis G.B. (1969) *One-dimensional two-phase flow*, McGraw-Hill, New York.
- Wilson I.D. (2004) Gas-Liquid Contact Area of Random and Structured Packing, *PhD Thesis*, University of Texas, Austin.

Manuscript accepted in May 2013

Published online in April 2014

Copyright © 2014 IFP Energies nouvelles

Permission to make digital or hard copies of part or all of this work for personal or classroom use is granted without fee provided that copies are not made or distributed for profit or commercial advantage and that copies bear this notice and the full citation on the first page. Copyrights for components of this work owned by others than IFP Energies nouvelles must be honored. Abstracting with credit is permitted. To copy otherwise, to republish, to post on servers, or to redistribute to lists, requires prior specific permission and/or a fee: request permission from Information Mission, IFP Energies nouvelles, revueogst@ifpen.fr.